

Persistence of bioconvection-induced mixed layers in a stratified lake

Oscar Sepúlveda Steiner ^{1,*} Damien Bouffard ² Alfred Wüest ^{1,2}

¹Physics of Aquatic Systems Laboratory, Margaretha Kamprad Chair, Institute of Environmental Engineering, École Polytechnique Fédérale de Lausanne, Lausanne, Switzerland

²Eawag, Swiss Federal Institute of Aquatic Science and Technology, Surface Waters – Research and Management, Kastanienbaum, Switzerland

Abstract

In situ observations of biophysical interactions in natural waters typically focus on physical mechanisms influencing biological activity. Yet, biological activity can also drive physical processes in aquatic environments. A community of photoautotrophic, motile and heavy bacteria—*Chromatium okenii*, which requires light, sulfide, and anoxic conditions to perform anoxygenic photosynthesis, accumulates below the chemocline of the meromictic Lake Cadagno (Switzerland). Upward vertical migration drives bioconvection, which modifies the physical environment of the bacteria-populated water to create a deep and homogeneous mixed layer of up to 1 m thickness. Continuous convection within the mixed layer and diapycnal diffusivity from its adjacent stratified surroundings determine ecologically relevant gradients. The daytime vertical migration that induce convective instabilities is well-established. It consists in bacteria swimming upward towards light and accumulating at the upper part of the anoxic layer, leading to a locally-unstable density excess. However, nocturnal activity has not yet been analyzed. An intensive 48-h survey was conducted in August 2018 using standard and microstructure profilers, as well as a moored high-resolution current meter coupled with temperature and turbidity sensors deployed across the mixed layer depth. This survey revealed a persistent mixed layer also during nighttime hours. Using a mixed layer shape model, vertical velocity observations and turbulent dissipation estimates, we conclude that photoautotrophic bacteria continue their vertical migration at night. This nocturnal activity thereby drives “dark bioconvection” and maintains the subsurface mixed bacterial layer in Lake Cadagno throughout the diel cycle.

The long-standing description of natural waters assumes that the physical environment influences biogeochemical processes to generate specific ecological niches. Hydrodynamically driven enhancement of primary production (Weiss et al. 1991; Oschlies and Garçon 1998; Dufois et al. 2016) and formation of plankton spatial structures (Abraham 1998; Ng et al. 2011; Lévy et al. 2018), such as thin layers (Steinbuck et al. 2009a; Durham and Stocker 2012), are typical examples of physical mechanisms that drive biological processes.

Nonetheless, biological activity can also influence and drive physical processes in aquatic systems. Examples of biophysical interactions affecting water characteristics at large spatial scales include planktonic modification of light absorption (Lorenzen 1972; Schanz 1985), which can lead to differential

heating (Sathyendranath et al. 1991; Strutton and Chavez 2004) and biogenic stratification (Weimer and Lee 1973; Culver 1977; Viaroli et al. 2018). At smaller scales, biologically-induced turbulence (Kunze et al. 2006; Lorke and Probst 2010; Simoncelli et al. 2018) is expected to drive water transport and mass exchange. The specific capacity of plankton to drive mixing has been demonstrated by laboratory experiments (Noss and Lorke 2014; Houghton et al. 2018). However, it still lacks conclusive in situ observations (Kunze 2019).

Bioconvection represents an intriguing example of bio-induced physical forcing (Hill and Pedley 2005; Bees 2020), in which heavy and motile microorganisms drive hydrodynamic changes in their immediate aquatic surroundings. This biophysical interaction has been extensively documented in laboratory settings using unicellular microorganisms (Bees and Hill 1997; János et al. 1998; Bearon and Grünbaum 2006). A recent study by Sommer et al. (2017) demonstrated that it also occurs in stratified natural waters.

Such biological phenomena leave specific, yet subtle physical traces in the aquatic environment. If those traces are

This is an open access article under the terms of the Creative Commons Attribution License, which permits use, distribution and reproduction in any medium, provided the original work is properly cited.

Additional Supporting Information may be found in the online version of this article.

sufficiently prominent, we attain the possibility to observe and investigate the original biological process by following its physical effects. This study documents bacteria-driven bioconvection in a lake by connecting several physical effects caused by motile, photoautotrophic sulfur *Chromatium okenii* communities. Lake Cadagno, a small alpine and meromictic lake in the Swiss Alps, provides an ideal natural laboratory. It hosts abundant photoautotrophic bacteria that create a homogeneous mixed layer (ML; Fig. 1). The goal of this study is to infer bacterial migration activity based on the bio-induced convective mixing characteristics of the water layer they inhabit. Specifically, using physical measurements, we sought to elucidate whether these bacteria remain active at night (Sepúlveda Steiner et al. 2019).

In this paper, we analyzed the persistent development of a bioconvective ML in Lake Cadagno during daytime and nighttime hours using an intensive 48-h field campaign. Specifically, we used (1) vertical microstructure profiles to evaluate the competing effects of bacteria-induced convection and turbulent diffusion adjacent to the bacterial layer and (2) temperature and velocity at different spatial and temporal scales to explain maintenance and persistence of the ML below the chemocline of Lake Cadagno throughout the diel cycle. Ultimately, this study

should motivate the use of physical observations to infer biological processes.

Bioconvection in Lake Cadagno

Study site

The study site, Lake Cadagno (Fig. 2; 46°33'3.13"N, 8°42'41.51"E) is located in the Swiss Alps at 1920 m asl. This small alpine lake has a maximum depth of 21 m and a surface area of 0.26 km². Deep, ion-rich, subaquatic inflows (Del Don et al. 2001) lead to permanent stratification and qualify Lake Cadagno as a crenogenically meromictic lake (Boehrer and Schultze 2008). The stratified water column exhibits a chemocline separating the oxygen-rich upper layer (top ~10 m) from the anoxic and sulfide-rich deep-water (deepest ~10 m).

Lake Cadagno freezes approximately from end-October to mid-May (with a thick snow cover) and remains stratified (thermally and by salinity) during this period. After the ice melts, diverse phototrophic sulfur bacteria form a layer at the oxic-anoxic transition, which gradually expands (Danza et al. 2018). This layer is composed by a community of purple-sulfur and green-sulfur bacteria (Schanz et al. 1998; Tonolla et al. 1999), of which *C. okenii* is the largest, the most abundant in biomass and, most importantly, the sole motile. During early summer and when *C. okenii* concentrations are

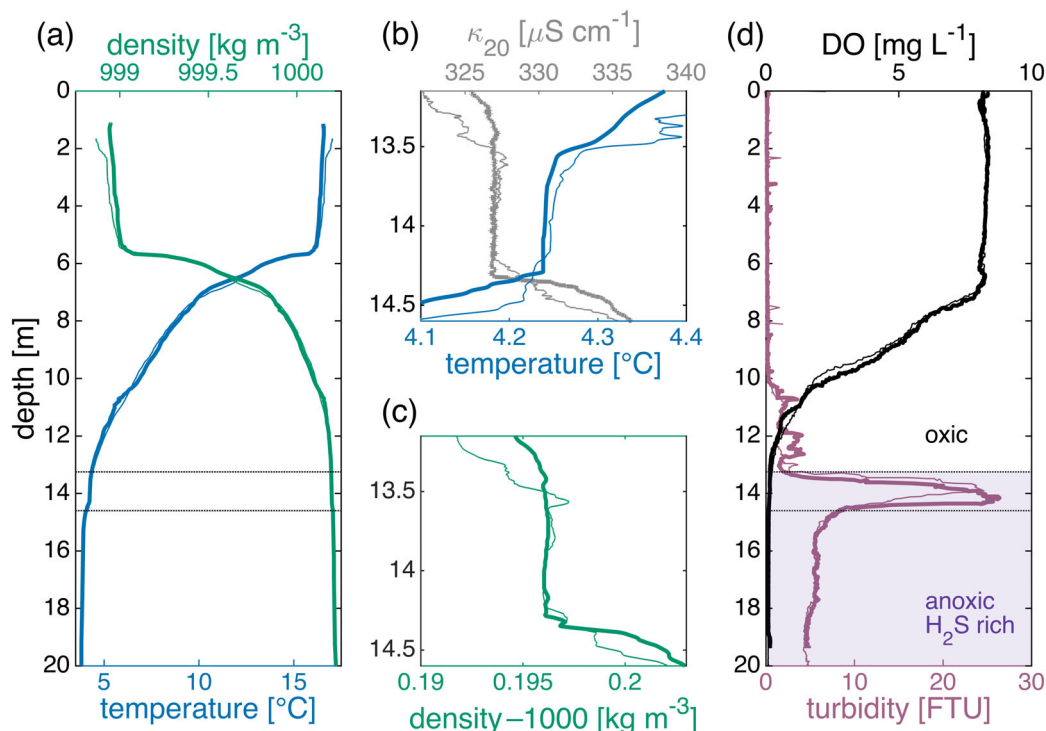


Fig 1. Comparison of day–night profiles. Night profile: 15 August 2018 21:00 (thin lines), and day profile: 16 August 2018 13:00 (thick lines). (a) Profile of water density (green) and temperature (blue; measured with a VMP-500 microstructure profiler). (b) and (c) Enlargement of profiles between dotted black lines in (a) that exhibit the mixed layer (ML). Additionally, (b) shows profiles of conductivity normalized to 20°C (κ_{20} ; gray). (d) Profile of turbidity (purple) and dissolved oxygen (DO; black) measured with a Sea & Sun CTD profiler. Dotted black lines, as in (a), show the turbidity peak associated with bacteria at the depth of the ML as highlighted in (b) and (c).

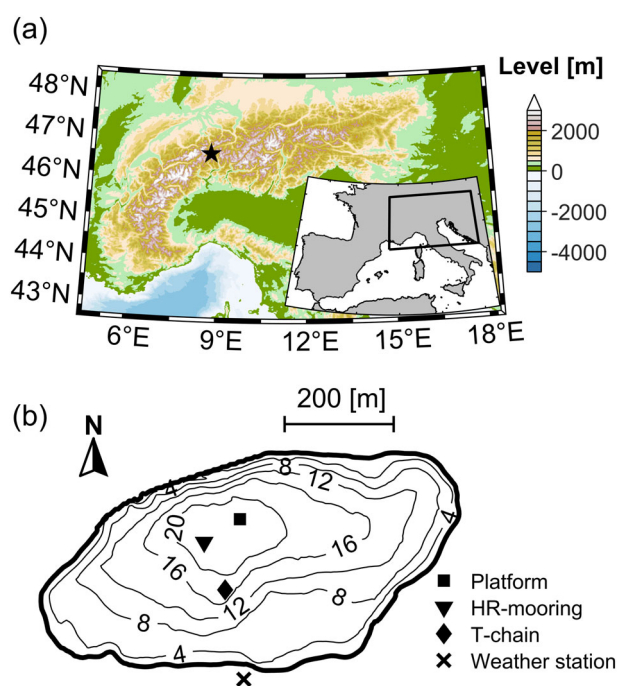


Fig 2. Study site location. **(a)** Map of the European Alps. The star denotes the location of Lake Cadagno. **(b)** Lake Cadagno bathymetry (depth isolines in m) with location of the platform (profiles), moorings and weather station.

sufficient, a ML forms within the bacterial layer depth range and remains, depending on the weather, until mid-September. The sulfur bacteria layer, although weakened, remains until the lake surface freeze.

Bioconvection in natural environments

Bioconvection induced by unicellular organisms develops when the density of motile cells exceeds that of ambient water and their local concentration reaches critical levels for determining the density of the water column they populate. These conditions create locally unstable density gradients. In order to sustainably maintain a consistent generation of convective plumes, cells must accumulate in a confined layer and perform net upward motion. Conditions limiting vertical migration of cells above the layer of accumulation are also necessary for its confinement (Sommer et al. 2017).

The photoautotrophic sulfur bacteria *C. okenii*, inhabits mainly the zone below the chemocline of Lake Cadagno. These microorganisms are denser than water ($\rho_B \approx 1150 \text{ kg m}^{-3}$) and capable of upward motility. Hydrological, morphological and geochemical characteristics of Lake Cadagno are favorable to meet the above-described conditions for bioconvection, particularly, those of the chemocline. During summer, *C. okenii* find ideal conditions of sunlight and H_2S below the chemocline (Schanz et al. 1998), where they can grow and accumulate at high concentrations ($10^5\text{--}10^6 \text{ cells mL}^{-1} = 10^{11}\text{--}10^{12} \text{ cells m}^{-3}$) in the oxic–anoxic transition (Danza et al. 2017; Sommer

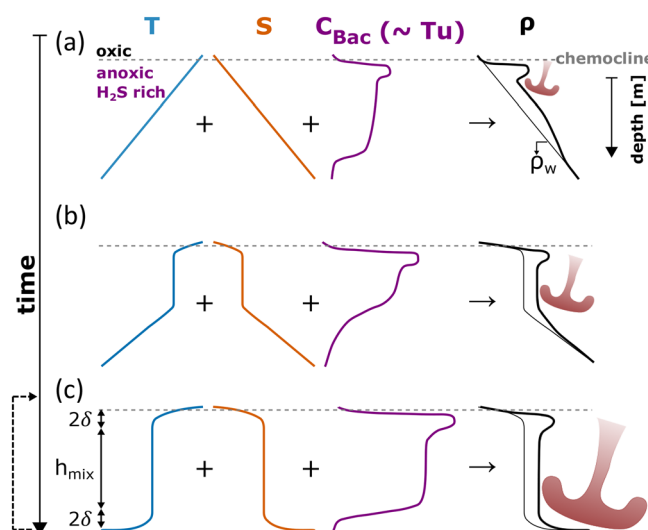


Fig 3. Bioconvective mixed layer (ML) formational stages: **(a)** initial, **(b)** intermediate, and **(c)** fully developed ML. Presence of high bacterial concentration C_{Bac} (m^{-3}), well-correlated with turbidity (Tu ; Fig. S1), increases the density of the water–bacteria mixture, exceeding the water density (ρ_w ; function of temperature and salinity). The water density plus the bacterial density contribution (water–bacteria mixture) is represented as $\rho_w + \rho_{\sigma\xi}C_{Bac}$ with ξ (m^3) representing the *C. okenii* density coefficient and ρ_o the reference density. Upward migrating bacteria accumulate at the oxic–anoxic interface and thereby cause unstable density profiles, which drive convective plumes (red mushroom-shaped feature).

et al. 2017). Their vertical distribution in the layer they inhabit is well correlated ($R^2 = 0.96$) with turbidity values (Fig. S1 in the Supporting Information). This correlation allows for vertical localization of bacteria. Light at the oxic–anoxic interface is more intense than at the bottom of the bacterial layer (Fischer et al. 1996), which motivates their continuous upward migration. Yet, above the chemocline, the presence of oxygen (Fig. 1d) limits their habitat, since anoxygenic photosynthesis requires anoxic conditions (Tonolla et al. 1999; Danza et al. 2017).

The upward migration of *C. okenii* towards the chemocline generates unstable density profiles of the water–bacteria mixture. This initiates convective mixing that generates a ML. Once established, convection allows the bacterial community to access sunlight from above and sulfide from below (Fig. 1c). The formation mechanism of MLs, starting with a stratified water column early in the season, is depicted in Fig. 3. Development of such MLs has been previously described using direct numerical simulations (DNS; Sommer et al. 2017). Once the ML is formed, the continuous bacterial upward migration sustain convection–diffusion competition (Sepúlveda Steiner et al. 2019) between the ML and its adjacent stratified waters above and below. This determines the ML vertical structure (Fig. 3c). Additionally, convection sharpens the gradient of H_2S through the base of the ML, which enhances its upward flux, thus contributing to the maintenance of bacteria.

Table 1. Details for sensors deployed on T-chain and HR-mooring (Fig. 1).

| Station | Instrument | Accuracy | Time response (s) | Sampling frequency (Hz) | Depths (m) |
|------------|-------------------------------------|--|-------------------|-------------------------|--|
| T-chain | RBRsolo T | $\pm 0.002^{\circ}\text{C}$ | ~ 1 | 0.1 | 0.25, 0.5 |
| | RBR TR-150 | $\pm 0.002^{\circ}\text{C}$ | ~ 1 | 0.1 | 0.75, 1.0 |
| | RBRconcerto ³ Tx | $\pm 0.005^{\circ}\text{C}$ | ~ 30 | 0.2 | 0.25, 0.5, 0.75, 1.0, 1.25, 1.5, 2.0, 2.5, 3.0 4.9, 5.0, 6.0, 7.0, 8.0, 9.0, 10.0, 11.0, 12.0, 13.0, 14.0, 15.0, 16.0 17.0 [mab] |
| HR-mooring | Nortek Aquadopp HR profiler (2 MHz) | $\pm 1\%$ of measured values $\pm 5 \text{ mm s}^{-1}$ | – | 0.5 | Installation: 14.5 Measurements: 11.9 to 14.0 m; 0.02 m bins |
| | RBRsolo T | $\pm 0.002^{\circ}\text{C}$ | ~ 1 | 2 | 12.0, 12.7, 12.9, 13.1, 13.8 |
| | RBRsolo Tu/Seapoint | – | 0.1 | 0.1 | 12.0*, 12.9, 13.8 |
| | Turbidity sensor | – | 0.1 | 0.1 | 12.0*, 12.9, 13.8 |
| | PME MiniDOT | $\pm 0.3 \text{ mg L}^{-1}$ | 30 | 0.02 | 12.0, 12.9, 13.8 |

Abbreviation: mab, meters above the bottom.

*Sensor did not record.

Up to this point, bioconvection in Lake Cadagno has been attributed to upward migration of *C. okenii* seeking light below the chemocline in order to optimize anoxygenic photosynthesis. This process explains the presence of a ML during daytime hours. Nevertheless, Sepúlveda Steiner et al. (2019) describe MLs that also occur at night. Three distinct hypotheses might explain the persistence of such a “dark ML”. First, background hydrodynamic processes in the lake may create or sustain the ML. Second, the decay timescale of the diurnal bioconvection may exceed the nighttime duration. Third, active upward migration of bacteria may also occur in the absence of light. By analyzing the ML evolution through two diel cycles, we evaluate these hypotheses and suggest that the third one is by far the most plausible.

Measurements and methods

Field measurements

The persistence of the bioconvective-induced ML in Lake Cadagno was intensively investigated during a 48-h survey in August 2018. To characterize the ML, microstructure and CTD profiles were performed from a platform situated in the open waters. In addition, an array of thermistors (T-chain) and a moored high-resolution (HR) current meter coupled with temperature sensors were installed at the ML depth (HR-mooring). Locations of the sampling platform and moorings are detailed in Fig. 2. Hydrodynamic measurements were complemented with meteorological observations obtained from a weather station (Vaisala instruments with a CR-6 Campbell Scientific data logger) installed on the south shore of the lake (Fig. 2). Weather conditions during the field campaign were warm with mild winds not exceeding 5 m s^{-1} . However, the observed ML was less prominent compared to previous years (Sommer et al. 2017; Sepúlveda Steiner et al. 2019).

Microstructure and CTD profiles

To resolve the ML and estimate turbulent parameters in the water column, we measured temperature and conductivity at high vertical resolution using a free-falling Vertical Microstructure Profiler VMP-500 (Rockland Scientific International, Canada). The profiler is equipped with two fast FP07 thermistors (nominal time response of $\sim 7 \text{ ms}$) and two fast SBE-7 conductivity microsensors mounted at the nose of the instrument and sampling at 512 Hz. Sommer et al. (2013) provides detailed description of the VMP-500 and its sensors. Profiles were measured at a sinking speed of $0.10\text{--}0.20 \text{ m s}^{-1}$ every 20 min during the 48-h survey. Slow falling speeds are required to resolve the temperature microstructure fluctuations that are later used to estimate turbulent dissipations. These measurements were complemented with profiles performed every hour using a Sea & Sun 75M CTD sampling at 8 Hz. In addition to the common CTD sensors, this profiler was equipped with pH, chlorophyll *a*, dissolved oxygen and turbidity sensors.

T-chain

A mooring equipped with an array of thermistors was installed close to the center of the lake (Fig. 2) to evaluate the temporal evolution of water column stratification. Table 1 lists thermistors characteristics and deployment depths.

HR-mooring

Hydrodynamic fluctuations in and around the ML were monitored with a high resolution mooring deployed below the chemocline ($\sim 12 \text{ m}$ depth). This equipment included a Nortek Aquadopp HR profiler (2 MHz) that faced upwards and measured current velocities (between 11.9 and 14.0 m depth; 0.02 m bins) at 0.5 Hz. The mooring devices also measured temperature, turbidity and dissolved oxygen using sensors installed at different depths above the Aquadopp. Table 1 lists

detailed settings, sensitivities and other information for sensors. Turbidity is used as a proxy to identify the location of the bacterial layer (e.g. Egli et al. 2004). Although we successfully collected data within the bacterial layer, inaccurate observations of the lake bottom depth caused the mooring to be deployed 0.6 m higher than intended. HR-mooring measurements below the bacterial layer are therefore not available.

Convection-diffusion competition

Convectively driven MLs developing in a stably stratified section of the water column are subject to background shear-turbulence that smooth them via diapycnal mixing with the stratified surroundings. In this paper, this limiting effect is referred to as convection-diffusion competition. We used the symmetric diffusive-shape model of Sepúlveda Steiner et al. (2019) to interpret convection-diffusion competition within the measured ML temperature profiles. The model (Φ_T) was deduced from the 1D vertical diffusion equation and reads as follows:

$$\Phi_T(z) = \Delta T \left[\operatorname{erf} \left(\frac{\frac{h}{2} - (z - z_0)}{\delta} \right) - \operatorname{erf} \left(\frac{\frac{h}{2} + (z - z_0)}{\delta} \right) \right] + T_o - G_T(z - z_0) \quad (1)$$

where z is the depth coordinate (positive downwards) and z_0 represents the center of the ML. The model assumes an initial step-function of height h (m), temperature T_o , and symmetric step ΔT . The diffusive length $\delta = \sqrt{4K\tau}$ (m) defines the extent of the ML boundaries affected by the vertical background diffusivity K ($\text{m}^2 \text{s}^{-1}$), which forces a smooth transition to background stratification over a diffusive timescale $\tau = \delta^2/4K$ (s). The additional term G_T describes the slope of the ML and has a fitting purpose only (Sepúlveda Steiner et al. 2019). The ML thickness h_{mix} is then given by:

$$h_{\text{mix}} = h - 4\delta \quad (2)$$

Lower δ values relate to sharp transitions from ML to surrounding water and therefore to strong convective ML activity relative to turbulent background diffusivity. Higher δ values indicate weak convection relative to background turbulent diffusion.

A bounded nonlinear fitting method was used to estimate ML model (Φ_T) parameters from temperature microstructure profiles. After fitting, only Φ_T with a coefficient of determination $R^2 > 0.75$ and a ML thickness $h_{\text{mix}} > 0.2$ m were considered for further analysis. Initial values and boundary conditions were the same as those provided in Sepúlveda Steiner et al. (2019). An equivalent procedure for analysis of turbidity profiles is given in the Supporting Information (Text S1 and Fig. S2).

Data analysis

Density calculations and water column stability

For this particular study, accurate estimates of water density (ρ_w) are required. We calculated ρ_w following Wüest et al.

(1996) and using the ionic water composition of Lake Cadagno. Expressed as a function of temperature (T) and salinity (S), ρ_w can be represented as:

$$\rho_w(T, S) = \rho_w'(T) + \beta S \quad (3)$$

where $\rho_w'(T) = 999.84 + 6.55 \times 10^{-2} T - 8.56 \times 10^{-3} T^2 + 5.94 \times 10^{-5} T^3$ is the T -dependent water density and $\beta = 0.96 \times 10^{-3} \text{ kg g}^{-1}$ is the haline contraction coefficient for Lake Cadagno water. Salinity is obtained using the expression $S = \alpha \kappa_{20}$, where $\alpha = 0.72 \times 10^{-3} \text{ kg m}^{-3} (\mu\text{S cm}^{-1})^{-1}$ is Lake Cadagno's ion-specific conductivity to salinity factor (Uhde 1992) and $\kappa_{20} (\mu\text{S cm}^{-1})$ is conductivity normalized to 20°C. A temperature-salinity diagram (Fig. S3), which constrains bacterial ML location, was used to estimate water density based on temperature only given HR-mooring data ($\rho_w = -0.026T + 1000.3$; for $3.8 \leq T \leq 4.5$). The term $\rho_w(T, S)$ represents the density of water only, without bacteria. The water-bacteria mixture density can be represented as:

$$\rho = \rho_w + \rho_o \xi C_{\text{Bac}} \quad (4)$$

where C_{Bac} is the bacterial concentration (m^{-3}), $\xi = 3.7 \times 10^{-17} \text{ m}^3$ is an estimated *C. okenii* density coefficient (Sommer et al. 2017) and $\rho_o = 1000 \text{ kg m}^{-3}$ is the reference density. This expression is used to evaluate profiles of water-bacteria mixture (Fig. S4) and to discuss general results of the 48-h survey.

The water column stability, is accounted through the buoyancy frequency $N^2 = g \rho_o^{-1} \partial \rho_w / \partial z$ (s^{-2}), where $g = 9.81 \text{ m s}^{-2}$ and z is the depth coordinate (positive downwards). The density gradient, $\partial \rho_w / \partial z$, is obtained through linear fitting of ρ_w in the vertical segment of interest.

Turbulent quantities and diffusivity

Temperature microstructure profiles were used to estimate rates of turbulent kinetic energy dissipation, ε , the Thorpe scale of overturns (Thorpe 1977) and turbulent diffusivities. These were estimated for the whole water column and within the ML and its adjacent waters (ML background).

Turbulent dissipation estimates, ε (W kg^{-1}), were obtained by fitting the Batchelor (1959) spectrum to the measured spectra of temperature gradient fluctuations. This procedure used a maximum likelihood spectral fitting method (Ruddick et al. 2000) and a correction by Steinbuck et al. (2009b) to calculate the smoothing rate of temperature variance, χ_θ ($^\circ\text{C}^2 \text{s}^{-1}$). Dissipation estimates obtained from poorly resolved spectra and those which did not comply with Batchelor fitting, were discarded according to likelihood and mean absolute deviation criteria proposed by Ruddick et al. (2000). For temperature microstructure, the detection floor of ε is in the range of 10^{-12} to $10^{-11} \text{ W kg}^{-1}$ (Luketina and Imberger 2001; Steinbuck et al. 2009b). Following Sepúlveda Steiner et al. (2019), turbulent dissipation estimates in the ML (ε_{ML}) were

obtained using the microstructure segment defined by h_{mix} that results from Φ_T -fitting.

Mixing is quantified following the diapycnal diffusivity model given in Osborn and Cox (1972). This model uses χ_θ estimates by applying:

$$K_{OC} = \frac{\chi_\theta}{2 \left(\frac{\partial T}{\partial z} \right)^2} \quad (5)$$

where $\partial T / \partial z$ is the slope obtained through linear regression of T in the vertical segment of interest. This provides diffusivity estimates for the whole water column since χ_θ can be directly estimated by integrating the temperature microstructure spectra. In particular, diffusivity estimates in the ML background (hereafter K_B) were derived from segments 1.5 m above and below h_{mix} .

We chose the Osborn and Cox (1972) model because, unlike Osborn's (1980) model, it does not require the usage of a diapycnal mixing coefficient, Γ . However, by comparing both models in the ML background depth range, we obtained $\Gamma = 0.15$ (Fig. S5). This is in agreement with diffusivities obtained by means of energy budget and dye tracer experiments for the interior of small- to medium-sized stratified lakes (Wüest et al. 2000).

Turbulent quantities and diffusivity often exhibit lognormal character. Statistical analyses therefore used a maximum likelihood estimator (mle) for a lognormal distribution (Baker and Gibson 1987). This reduced the influence of extreme values and provided ad-hoc estimates of statistical variability through the intermittency factor $\langle \sigma_{mle}^2 \rangle$, which is denoted by pointy brackets, $\langle \cdot \rangle$, throughout the article.

Buoyancy flux and convective velocity

The buoyancy flux within the ML, a key parameter for characterizing convection, was calculated following Sepúlveda Steiner et al. (2019) as:

$$J_b^{ML} = \eta_{bc} \cdot \epsilon_{ML} \quad (6)$$

where ϵ_{ML} is the ML dissipation and $\eta_{bc} = 0.55$ is the bioconvective mixing efficiency used in Sepúlveda Steiner et al. (2019) as deduced from DNS results reported by Sommer et al. (2017). Convective mixing efficiencies have been theoretically demonstrated to lie in the range of 0.5–1 (Davies Wykes et al. 2015). The vertical convective velocity (w^*) can then be characterized by Deardorff (1970) as:

$$w^* = (J_b^{ML} h_{mix})^{1/3} \quad (7)$$

where h_{mix} is the ML thickness. Finally, the convective time-scale is given by $\tau^* = (h_{mix}^2 / J_b^{ML})^{1/3}$.

Flow stability

The gradient Richardson number Ri_g (Turner 1973) was used to account for flow stability. This dimensionless number is defined as:

$$Ri_g = \frac{N^2}{S^2} \quad (8)$$

where $S^2 = (\partial u / \partial z)^2 + (\partial v / \partial z)^2$ is the square of the vertical current shear with u and v representing horizontal velocities. For shear flows wherein $Ri_g > Ri_g^c = 0.25$, buoyancy suppresses vertical displacements to maintain stable hydrodynamic conditions. For $Ri_g < Ri_g^c$, stratified shear flow can initiate instabilities and enhance vertical mixing (Ivey et al. 2008). Time series for Ri_g were obtained from the Aquadopp HR profiler data averaged over 5 min and vertically smoothed using a running mean among four vertical bins.

Results

Water column structure

This study sought to determine whether hydrodynamic factors create or sustain MLs as observed in Lake Cadagno. In summer, the Lake Cadagno water column consists of three distinct hydrodynamic zones (Figs. 1, 4a, S6). A 5-m thick surface layer (yellow zone in Fig. 4a), an extremely stable interior (5–12 m depth; orange to purple) and a weakly stratified deep layer (dark purple). In the interior, the T-chain measurements (Fig. 4a) indicated a temperature gradient of $1.4 \pm 0.1^\circ\text{C m}^{-1}$ and the CTD profile recorded a strong median stability of $N^2 \approx 1.1 \times 10^{-3} \text{ s}^{-2}$. This suggests that the strongly stratified interior isolates the bacterial layer at ~ 14 m depth from the surface layer. Therefore, this surface layer is not considered further. The weakly-stratified deep waters below the bacterial layer exhibited a temperature gradient of $0.08 \pm 0.03^\circ\text{C m}^{-1}$ with a low stability of $N^2 \approx 3.8 \times 10^{-5} \text{ s}^{-2}$. Taking the density profile presented in Fig. 1a into account and assuming a three-layer representation (Münich et al. 1992) with a wind-fetch length of 900 m, the first and second internal seiche mode periods yield approximately 2 and 7 h, respectively.

The strong stratification suppressed overturns and vertical mixing in the interior. The Thorpe scale (Fig. S6c) fell below the cm range indicating an extremely well sorted thermocline without overturns. Consequently, diapycnal diffusivity (Fig. S6d) was close to molecular, with a mle-mean of $1.5 \times 10^{-7} \text{ m}^2 \text{ s}^{-1}$ (3.4). By contrast, the water column showed enhanced mixing below 12 m depth. The average Thorpe scale was $L_T = 0.04 \pm 0.05 \text{ m}$ and diffusivity gave a mle-mean of $6.3 \times 10^{-5} \text{ m}^2 \text{ s}^{-1}$ (9.5) with strong intermittency.

The bacterial layer developed below the oxic–anoxic interface and was tracked using turbidity profiles (Figs. 1, S1). Time series of turbidity profiles (Fig. 4b) revealed a consistent peak in turbidity at ~ 14 m depth. We observed that the position

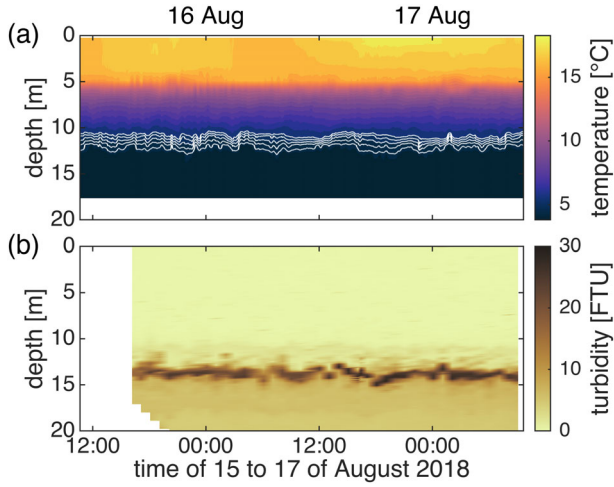


Fig 4. Water column conditions during the field campaign. **(a)** Temperature profiles continuously measured by the T-chain mooring. **(b)** Turbidity profiles measured with the Sea & Sun CTD at the sampling platform. White lines in **(a)** correspond to isotherms 4.5 (bottom), 4.75, 5.0, 5.25, and 5.5 °C (top). The dark color band in **(b)** indicates the bacterial layer at 14 m depth.

and thickness (expansion/contraction) of the turbidity layer oscillated vertically by ~ 1 m as a result of isothermal movements, which exhibited periodicities of 4.0, 1.7, and 0.6 h (Fig. S7a).

Mixed layer characteristics and evolution

During the August 2018 field campaign, we collected 142 temperature microstructure profiles using duplicated sampling (284 in total). Figure 5a provides an example of the temporal evolution of a typical ML temperature profile as collected on 15 August 2018. This is accompanied by a mid-day profile subjected to fitting to the ML-shape model (Φ_T ; Fig. 5b). From the total of 284 samples, 136 met the Φ_T -fitting procedure criteria. These allowed for direct deduction of h_{mix} and δ , represented as arithmetic means of 0.50 ± 0.22 m and 0.18 ± 0.09 m, respectively. Time series results of Φ_T (Fig. 5c) show mixed layer position (z_o) and h_{mix} throughout the 48-h sampling. The baroclinic displacements presented above seem to affect z_o and h_{mix} , however, for the analysis of bioconvective ML presented here, the role of internal waves is secondary.

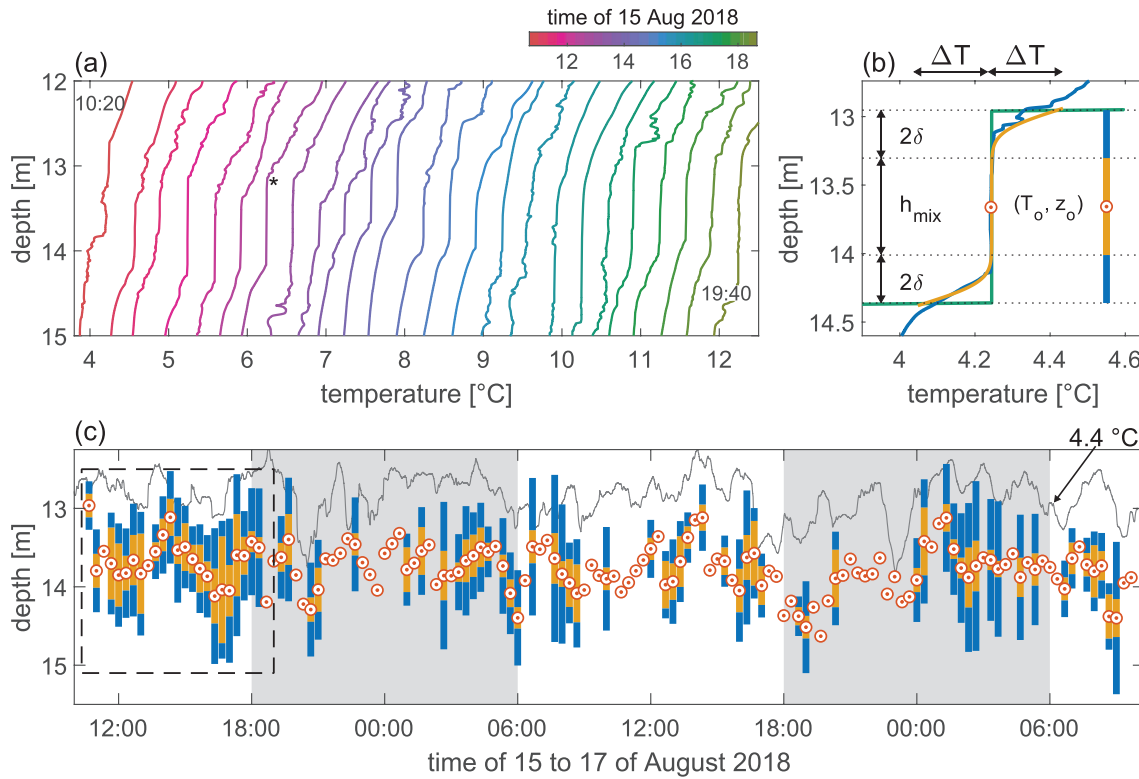


Fig 5. Time series of measured mixed layer (ML) profiles and ML-shape model (Φ_T) analysis. **(a)** Waterfall plot of measured MLs during 15 August 2018. An offset of 1°C h^{-1} was applied to separate the profiles. **(b)** Example of the ML-shape model showing a temperature profile (blue; *-marked profile in **(a)**) with its respective fitting (orange; $R^2 = 0.97$), initial step-like ML (green) and the definition of h_{mix} and δ following Sepúlveda Steiner et al. (2019). **(c)** Time series of Φ_T results. Orange and blue bars represent h_{mix} and 2δ as defined in **(b)**. Only profiles that meet the Φ_T -fitting criteria are considered. Bars represent averages of Φ_T results from the two fast thermistors mounted on the VMP. Profiles with only one sample meeting the criteria are also displayed. For reference, z_o (orange dotted circles) of discarded profiles are included. Gray areas represent nighttime for the 48-h measurement period. The gray line depicts the 4.4°C isotherm obtained from the HR-mooring. The dashed box corresponds to the measurements displayed in **(a)**.

Table 2. Characteristics of the observed convective ML in Lake Cadagno during August 2018. Results are shown separately for daytime and nighttime periods. Data from this field campaign was also presented in Sepúlveda Steiner et al. (2019) and results are similar except for K_B , which is estimated following Osborn and Cox (1972).

| Parameter measured | Units | All | Daytime | Nighttime |
|--|----------------------|-----------|-----------|-----------|
| Thickness of mixed layer (h_{mix}) [†] | m | 0.50±0.22 | 0.53±0.24 | 0.46±0.18 |
| Diffusive boundary length-scale (δ) [†] | m | 0.18±0.09 | 0.17±0.09 | 0.21±0.08 |
| Mixed layer stability (N^2_{ML}) [†] | $10^{-5} s^{-2}$ | 0.54±1.38 | 0.56±1.59 | 0.52±1.01 |
| Background stability (N^2_B) [†] | $10^{-5} s^{-2}$ | 7.9±1.5 | 7.9±1.6 | 7.8±1.4 |
| Dissipation rate in the mixed layer (ϵ_{ML}) [‡] | $10^{-10} W kg^{-1}$ | 4.3 (2.7) | 6.9 (2.7) | 1.4 (1.9) |
| Convective plume velocity (w^*) [†] | mm s ⁻¹ | 0.37±0.25 | 0.43±0.27 | 0.27±0.17 |
| Convective timescale (τ^*) [†] | min | 30±19 | 27±20 | 35±17 |
| Background diffusivity (K_B) [‡] | $10^{-6} m^2 s^{-1}$ | 3.4 (1.9) | 3.6 (1.9) | 3.3 (2.0) |

[†]Results are reported as arithmetic mean ± standard deviation.

[‡]Statistics of the rate of dissipation and diffusivity are reported following Baker and Gibson (1987) given by mle-mean for lognormal distribution and intermittency factor (σ^2_{mle}) inside $\langle \rangle$ brackets.

Mixed layers were observed during both daytime and nighttime hours. Table 2 and Fig. 6a,b show a statistical comparison of ML characteristics between these two periods. While h_{mix} was 13% larger during daytime, δ was 19% larger during nighttime. This finding indicates more vigorous convection during daytime coupled with more effective diffusion-driven smoothing (enhanced δ) at night (Sepúlveda Steiner et al. 2019). Analysis of the variability in the vertical profiles performed by stretching/compressing the MLs to a normalized scale (Fig. 7a,b), however, showed only subtle shape differences between daytime and nighttime. Consistent with these results, ML stability estimates (N^2_{ML} ; Table 2) showed only minor variation. This suggests that the differences between daytime and nighttime estimates are not statistically significant.

Microstructure data within the MLs and their adjacent regions were analyzed according to the methods presented above (Fig. 6). Here we focus on distributions of dissipation rates (ϵ_{ML}) in the ML, convective velocity scale (w^*) and background diffusivity (K_B). The histograms in Fig. 6 also distinguish daytime and nighttime values. Table 2 summarizes the statistics from this analysis and highlights the overall low energy level in the ML (mle-mean $\epsilon_{ML} = 4.3 \times 10^{-10} W kg^{-1}$ (2.7)). In general, daytime profiles exhibited enhanced convection compared to that observed in nighttime profiles. Quantitatively, ϵ_{ML} and w^* differed by factors of 4.9 and 1.6, respectively. Regions of the water column adjacent to the ML consistently showed an average diffusivity of $\overline{K_B} = 3.4 \times 10^{-6} (1.9) m^2 s^{-1}$, or one order of magnitude higher than thermal molecular diffusion. This value is in reasonable agreement with the diapycnal diffusivity estimate of $K_{W94} = 1.6 \times 10^{-6} m^2 s^{-1}$ reported from a tracer release experiment at the same depth in Lake Cadagno (Wüest 1994). Diffusivity was slightly more intense during the daytime evident from a factor 1.1 difference between daytime and nighttime measurements (Table 2).

Day–night comparison of turbidity profiles

Additional analysis of turbidity profiles was used to investigate physical signatures of bioconvection (Fig. 7c,d). Measured turbidity profiles (43 in total) are separated for daytime and nighttime periods (25 and 18 profiles, respectively). The bacterial layer appears as a consistent peak (>10 FTU) at around 14 m depth (ranging from 13 to 15 m) with a maximum not exceeding 30 FTU. The upper boundary of the layer appears as a slightly sharper transition than its lower boundary. This feature represents the oxic-anoxic transition since dissolved oxygen prevent further vertical migration of the bacteria, which leads to a sharper upper boundary. The more gradual lower transition likely arises from higher turbulent diffusion (Fig. S6d) and because bacteria can sink beyond the ML zone. Vertical displacements affect the turbidity peak position (Fig. 4b), however Fig. 7c,d show that these remained in a more stable position during nighttime.

Isopycnal-averaged profiles were used to analyze turbidity peaks without the influence of baroclinic displacements (Fig. 7c,d; thick black lines). This analysis reveals subtle shape differences between daytime and nighttime mean turbidity profiles and offers no indication of bacteria sinking at night. Additionally, turbidity profiles were further analyzed by using a turbidity shape model (*Tu*-model; Text S1 and Fig. S2). Although this analysis resulted in h_{mix} estimates ~2-times smaller than those generated by the ML-shape model (explanation in Text S1), the *Tu*-model daytime and nighttime parameters do not show significant statistical differences (Table S1). Taken together, turbidity profile analyses suggest a net energy input to maintain the peak characteristics. We interpret this input to represent bacterial upward migration in the water column during both, daytime and nighttime.

HR-mooring measurements

Fluctuations in velocity measured by the HR-mooring equipment provide further confirmation of bacteria-induced

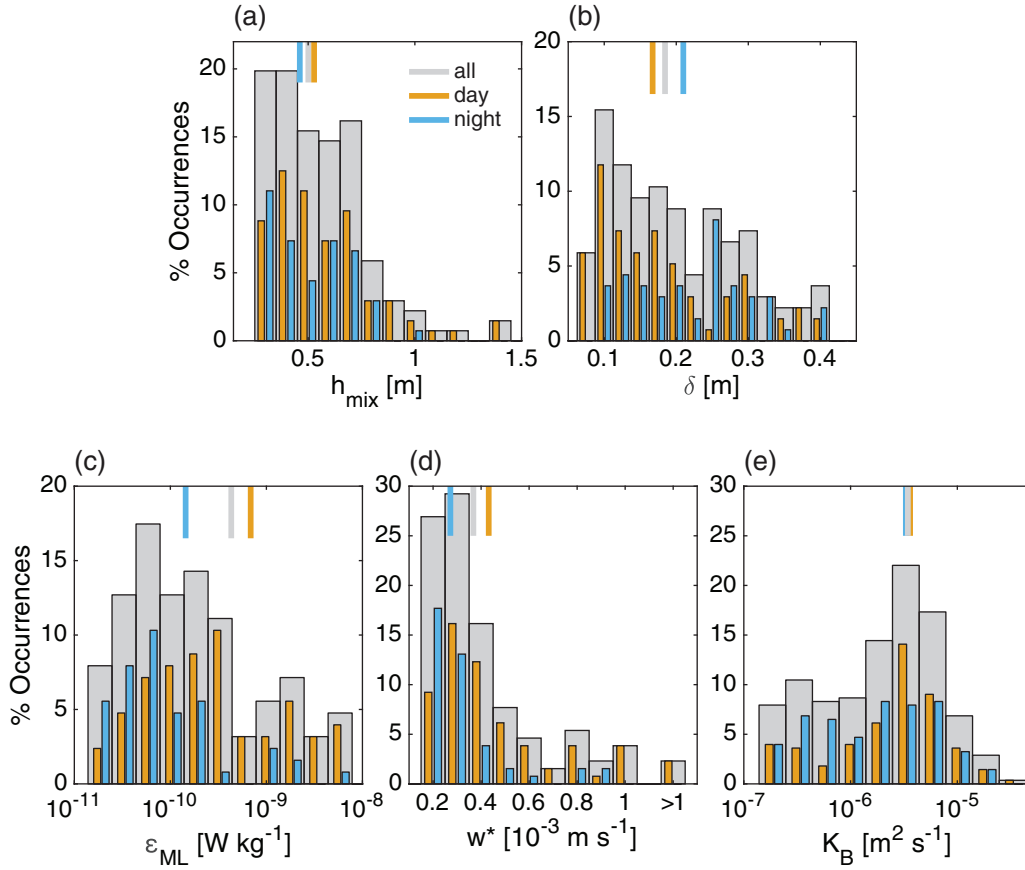


Fig 6. Statistical distribution of mixed layer (ML) characteristics. **(a)** ML thickness h_{mix} , **(b)** diffusive length scale δ related to ML boundaries, **(c)** dissipation ϵ_{ML} in the mixed layer, **(d)** convective velocity scale w^* within the ML, and **(e)** background diapycnal diffusivity K_B (gray bars) following Osborn and Cox (1972). Histograms are presented for the whole 48-h sampling (gray bars) and also for separate daytime (orange bars) and nighttime (blue bars) periods. Vertical lines at the top of each panel correspond to the arithmetic mean in **(a)**, **(b)**, and **(d)** and to the mle-mean (Baker and Gibson 1987) in **(c)** and **(e)**.

convection. Detailed time series of wind, dissolved oxygen and currents are presented in Fig. S8. Here, we focus on turbidity, vertical velocities and estimates of the gradient Richardson number Ri_g (Fig. 8).

Measured vertical velocities ranged between -1.5 and $+1.5 \text{ mm s}^{-1}$ (Fig. 8b; positive upwards). Continuous changes of the sign of velocity values (from red to blue and vice versa) below the 4.4°C isoline indicate convective activity. Spectral analysis of vertical velocity (Fig. S7b) also detected marked oscillations with periods of 25–30 min. As these periodicities are considerably smaller than the seiche periods but comparable to convective timescale values, τ^* (Eq. 7), of 30 ± 19 min (Table 2), we interpret them as a signature of convection.

Turbidity sensors mounted on the HR mooring provided estimates of the ML position that were subsequently used to analyze convective velocity fluctuations. Turbidity time series (Fig. 8a) show strong variability (coefficient of variation of 0.87 for the central sensor) indicating fluctuations in the vertical position of the bacterial ML. This result agrees with the T-chain and profiling results. The turbidity sensor installed at

13.8 m depth was configured in auto-range mode. Unfortunately, the sensor sampled only within the 0–25 FTU range and failed to record higher values (Fig. 8a). The data were still adequate for identifying periods when the bacterial ML appeared at ~ 13.8 m depth with turbidities exceeding 10 FTU (Fig. 7c,d).

A statistical analysis of measured vertical velocities was performed to further validate microstructure-based estimates (w^* ; see Fig. 6d). To select vertical velocity data, which were reliably within the ML, we discarded data above the 4.4°C isotherm and beneath the lowermost turbidity sensor (13.8 m depth) for turbidities below 10 FTU (thick black line between Fig. 8c,d).

Figure 9a shows distributions of depth-averaged vertical velocity. This analysis was performed by detrending the depth-averaged velocity time series and separating them into upward and downward components. This process gave results strongly resembling half-normal distributions with arithmetic averages of $0.33 \pm 0.25 \text{ mm s}^{-1}$ and $0.35 \pm 0.28 \text{ mm s}^{-1}$ for upward and downward components, respectively. Downward

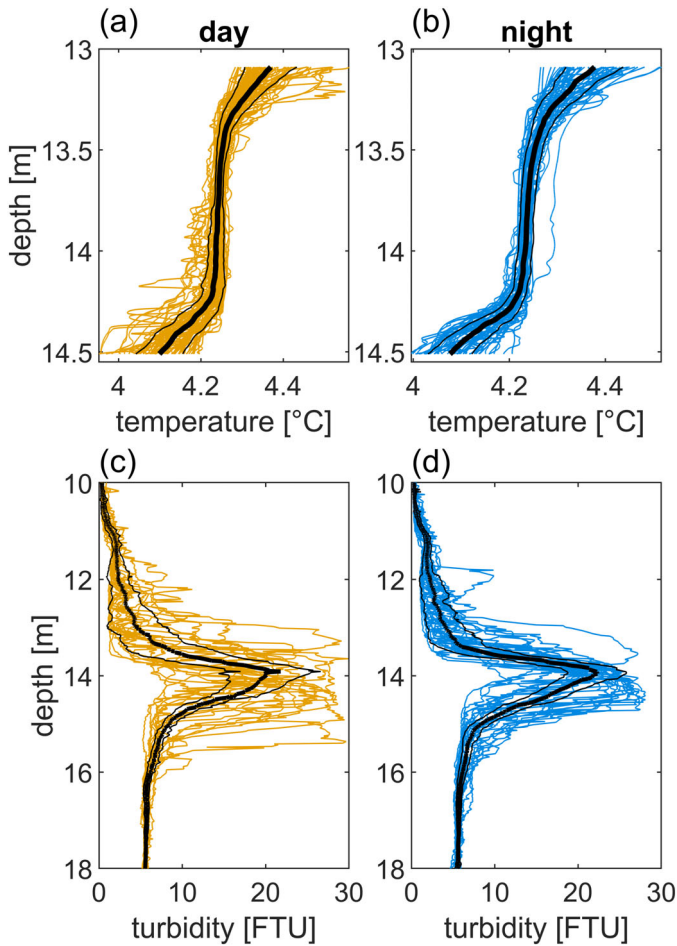


Fig 7. Comparison of temperature mixed layers and turbidity profiles measured during daytime and nighttime hours. **(a, b)** Stretched/compressed MLs separated for daytime and nighttime hours, respectively. Only profiles that meet the Φ_T -fitting criteria are considered. The thick and thin black lines represent arithmetic mean and standard deviation, respectively. **(c, d)** Measured turbidity profiles accompanied by their isopycnal-averages (black thick line) and standard deviations (thin black lines).

plumes exhibited slightly higher velocities, whereas upward plumes were more frequent (by 6%), particularly in the range $0.15\text{--}0.55\text{ mm s}^{-1}$. This directional asymmetry balances the mass flux budget (Jonas et al. 2003). Moreover, average velocities showed good agreement with microstructure-based estimates of w^* ($0.37 \pm 0.25\text{ mm s}^{-1}$). This represents further evidence of the convective nature of the ML observed in Lake Cadagno.

The same analysis is performed separately for daytime and nighttime periods (Fig. 9b,c). These periods show similar upward and downwards averages and asymmetric directional features. The distributions do not show considerable difference between daytime and nighttime values. Although w^* varies by 59% between daytime and nighttime hours (Table 2), the HR current measurements show only minor differences (<5%).

The Aquadopp HR current profiler recorded lateral current magnitudes of up to 10 mm s^{-1} (Figs. S8e,f). This information was used to account for flow stability by estimating Ri_g . The magnitudes of Ri_g suggest that shear is not capable of generating instabilities above the bacterial ML (Fig. 8c). However, values of $Ri_g < 0.25$ appeared primarily within the bacterial ML (below 4.4°C isotherm). This indicates that the reduced stratification due to the convective activity could sporadically favor shear-driven instabilities.

Discussion

The study focused on quantifying the physical characteristics of the bioconvective ML in Lake Cadagno over a 48-h period. It provides physical evidence of ML persistence throughout the daily cycle likely driven by bacterial activity.

Day–night cycle persistency. The bacteria layer remained mixed over the entire observation period regardless of light conditions (Figs. 5 and 7a,b). Small-scale analysis detected a noticeable decrease in turbulent dissipation at night ($\epsilon_{ML}^{\text{night}} / \epsilon_{ML}^{\text{day}} \approx 0.2$) indicating a decrease in convection. However, ML characteristics did not change significantly as demonstrated by $h_{\text{mix}} \approx 0.50 \pm 0.22\text{ m}$, a parameter that differs by only 15% between daytime and nighttime observations. The diffusive boundary transition of $\delta \approx 0.18 \pm 0.09\text{ m}$, as driven by adjacent diapycnal diffusivity ($\overline{K_B} = 3.4 \times 10^{-6}\text{ (1.9) m}^2\text{ s}^{-1}$), differed by $\sim 19\%$ between daytime and nighttime periods. Turbidity peak shape (Fig. 7c,d) and convective velocities (Fig. 9) also indicate that ML characteristics remained virtually unchanged throughout the day–night cycle.

Dissipation decay. To further elucidate whether bacteria actively migrate upward at nights, we analyzed the temporal evolution of turbulent dissipation in the ML (ϵ_{ML} ; Fig. 10a). We compared the observed decay in convective activity to the e-folding decay (Caldwell et al. 1997) expected to result from a sudden cessation of convection triggered by a drop in phototrophic activity. In our case, the e-folding decay is characterized by the convective timescale $\tau^* = 30 \pm 19\text{ min}$ (Table 2). This implies a 95% reduction of ϵ_{ML} (Fig. 10a) over a $\sim 1.5\text{ h}$ period ($3\tau^*$). However, the measured dissipation exhibited much slower decay than the e-folding predictions. Although the measured dissipation declines during nighttime, time series indicate a continuation of the bacteria-induced convection at night to maintain the ML.

Mixed layer thickness decay. Similarly, the temporal evolution of h_{mix} also records nighttime bacterial activity. A completely inactive ML would smooth out unhindered due to the action of eddy diffusivity in the adjacent water column. Figure 10b shows this scenario assuming a ML-model for two different levels of constant diffusivity (measured and molecular). Field estimates of diffusivity suggest smoothing of the $\sim 0.5\text{ m}$ thick ML takes $\sim 20\text{ min}$. Molecular diffusion

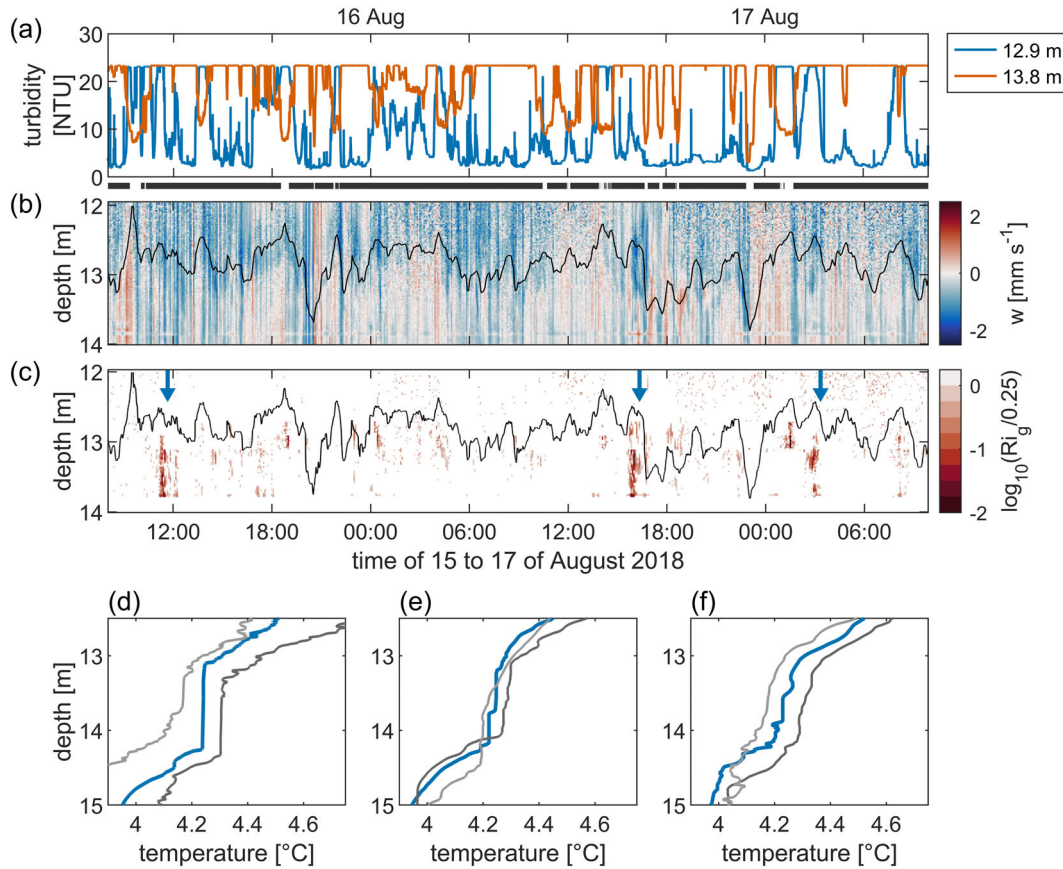


Fig 8. HR-mooring observations and gradient Richardson number (Ri_g) estimates. **(a)** Turbidity. **(b)** Vertical velocity component (w), measured with the Aquadopp HR profiler. Thick black line between panels **(a)** and **(b)** corresponds to measurement of turbidity at 13.8 m exceeding 10 NTU (i.e., measurement performed within the bacterial layer). **(c)** Gradient Richardson number (Ri_g) normalized by the critical value 0.25. The black lines in **(b)** and **(c)** correspond to the 4.4°C isotherm obtained from the HR-mooring. **(d, e, and f)** Three examples of temperature microstructure profiles for the ML and adjacent regions during periods of $Ri_g \leq Ri_g^c \approx 0.25$. Thick blue lines correspond to profiles performed at intervals indicated by blue arrows in **(c)**, same order. Profiles performed 20 min before (light gray; -0.05°C offset) and after (dark gray; +0.05°C offset) the $Ri_g \leq Ri_g^c$ event are provided to account for discrepancies between profiles and HR measurements. HR measurements were performed at ~50 m distance from the profiling platform.

suggest it could take 10 and 7 h for each of the two monitored nighttime periods. Comparison of measured h_{mix} with ML-model predictions also suggests that ML maintenance during nighttime hours requires active, upward bacterial migration to maintain the layer.

Role of stratification. Stratification plays a key role in ML maintenance. The lake interior exhibits a strong stratification ($N^2 \approx 1.1 \times 10^{-3} \text{ s}^{-2}$; Fig. S6a). Thorpe scales of overturn are extremely low (<1 cm; Fig. S6c) and diffusivities approach molecular rates ($1.5 \times 10^{-7} \text{ m}^2 \text{ s}^{-1}$ (3.4); Fig. S6d). Strong stratification counteracts background turbulence and its smoothing effects. The importance of this interplay becomes most evident when analyzing bacterial accumulation at the top of the ML (Fig. 3). A series of turbidity profiles measured in July 2017 (Fig. S9a,b) provide a compelling example of this feature. Using a numerical scheme to account for 1D vertical diffusion (Fig. S9c), we show that the background diffusivity would smooth out the turbidity profiles and disrupt the ML in

absence of active upward migration of bacteria. By comparison, a more energetic environment ($K_{ocean} \approx 10^{-5} \text{ m}^2 \text{ s}^{-1}$; Fig. S9d) would more rapidly vanish the bacterial layer due to strong background smoothing. Therefore, the mild background diffusivities in Lake Cadagno, which result from a resistance to diapycnal mixing imposed by the strong stratification, enable bacterial accumulation that in turn drives convection. Analysis of ML shapes showing gradient Richardson numbers below the critical value ($Ri_g^c \approx 0.25$) supports this interpretation (Fig. 8d,e,f). In these cases, buoyancy can no longer suppress vertical dislocations. Diffusivity and shear turbulence can then influence the ML shape, inducing enhanced smoothing and/or adjacent sheared layers.

Dark bioconvection. To perform upward migration and drive bioconvection during nighttime, *C. okenii* requires an energy source different from anoxygenic photosynthesis. Recently, Berg et al. (2019) reported on *C. okenii*'s ability to carry out aerobic sulfide respiration, independent of light, in

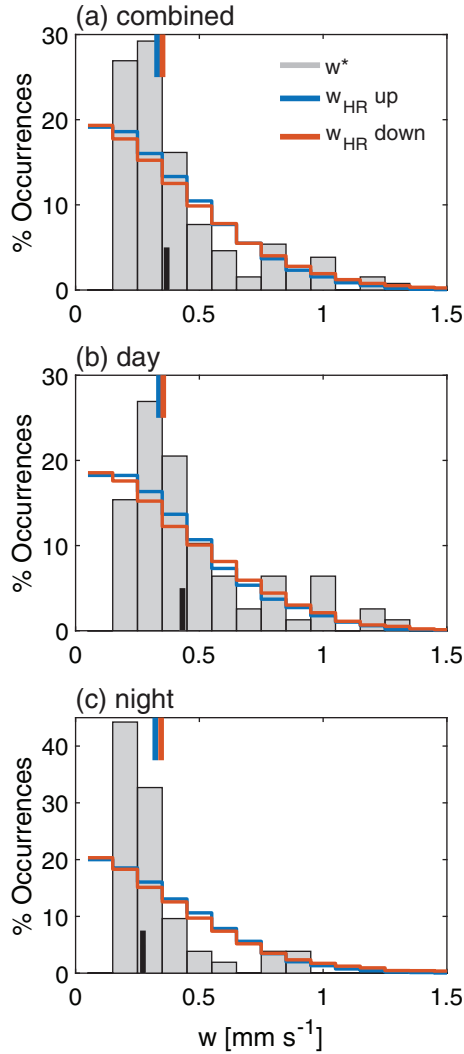


Fig 9. Comparison of depth-averaged vertical velocity (w) distributions within the ML with convective plume velocity. **(a)** Whole dataset (combined). **(b, c)** Daytime and nighttime sub-datasets, respectively. Gray bars corresponds to the ε -based convective plume velocity (w^* ; Deardorff 1970), whereas blue and red lines were obtained from the Aquadopp HR-mooring separated for upward and downward components, respectively. In each panel, the vertical bars correspond to arithmetic means following the same color-code with the exception of w^* , which is shown in black for better visibility.

the presence of nano-scale oxygen concentrations. Luedin et al. (2019) provided genetic evidence for dark chemolithotrophic oxidation of sulfur compounds by *C. okenii*. These metabolic pathways along with the presence of intracellular sulfur globules and energy storage molecules such as polyhydroxybutyrate (PHB; Luedin et al. 2019) or glycogen (Berg et al. 2019) in *C. okenii*, indicate the existence of a nighttime energy source crucial for bacterial motility. Chemotaxis, negative for oxygen and positive towards H_2S , is well described in *C. okenii* (Luedin et al. 2019). During nighttime, the weakening of convection and diffusivity-driven smoothing of the ML

may re-establish H_2S and oxygen gradients enabling bacteria chemotactic behavior. This provides a credible orientation mechanism for bacterial accumulation below the chemocline and subsequent generation of bioconvection despite the absence of light. Bioconvection may in turn improve the opportunities for microorganisms to access the trace amounts of oxygen needed to maintain a dark metabolism. Further research is needed to better characterize *C. okenii*'s range of metabolic processes and orientation behavior involved during the observed dark bacterial activity. The physical analysis presented in this paper does not resolve metabolic processes, but highlights several constraints regarding upward migration during nighttime hours.

Mixed layer formation timescale. Solely phototactic migration would imply that the ML forms every morning after sunrise. This would be due to the omnipresent effect of shear-induced eddy diffusion that smooths out the ML during nighttime (Fig. 10; Sepúlveda Steiner et al. 2019). If convective plumes within the ML represent a favorable environment for *C. okenii*, the time needed for their formation is critical given the ~ 12 h maximum duration of sunlight. To estimate this, it is necessary to analyze the energetics of ML formation (Fig. 3). Given a constant initial density gradient ($\rho_w(z) \sim \rho_o N_B^2 g^{-1} z$), the potential energy required to mix a h_{mix} -thick water column below the chemocline can be represented as:

$$PE = \int_{-\frac{h_{mix}}{2}}^{\frac{h_{mix}}{2}} \rho_w(z) g z \, dz = \int_{-\frac{h_{mix}}{2}}^{\frac{h_{mix}}{2}} \rho_o N_B^2 z^2 \, dz = \frac{1}{12} \rho_o N_B^2 h_{mix}^3 \quad (9)$$

where PE is in $J \, m^{-2}$ and the origin lies at the center of the resulting ML. Furthermore, the energy flux generated by upward bacterial migration can be expressed as $E_f = J_{net} \rho_o h_{mix}$ ($W \, m^{-2}$) with J_{net} as the net buoyancy flux for ML expansion. This can be modeled as $J_{net} = J_b^{ML} - J_b^B$, i.e., the difference between ML and background buoyancy fluxes, with $J_b^B = K_B N_B^2$. Finally, $\tau_{h_{mix}} = PE/E_f$ represents the timescale for generating a ML of thickness h_{mix} . Average values reported in Table 2 for daytime hours yield $PE = 8.2 \times 10^{-4} J \, m^{-2}$ and a $\tau_{h_{mix}} = 4.8$ h to form a 0.5 m thick ML. This result indicates that ML formation can take up a major fraction of one day. Given that the background smoothing effect remains active, our analysis suggests that the continuation of bioconvection at night represents a more energy-efficient strategy than forming the ML on a daily basis. However, for average nighttime conditions, no positive net buoyancy flux was achieved. This suggests that if nighttime convection occurs, it does so intermittently and it only contributes towards maintaining and not expanding the ML.

Vertical velocity scales relevant for *C. okenii*. During nighttime, *C. okenii* (density $\rho_B \approx 1150 \, kg \, m^{-3}$) would immediately

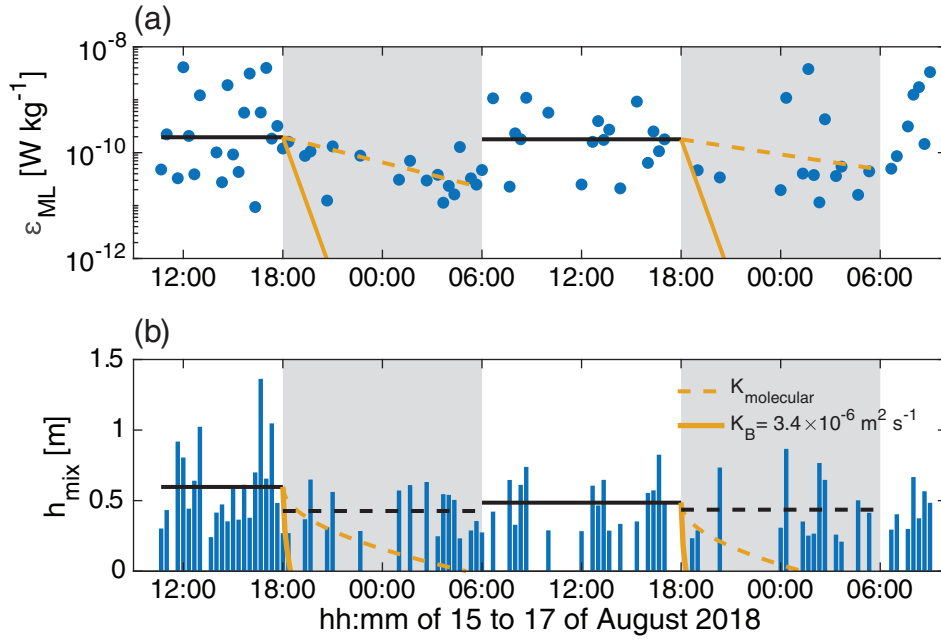


Fig 10. Temporal evolution of ML convective turbulence. **(a)** ML dissipation rate ε_{ML} (blue dots). Gray areas correspond to nighttime periods. The orange line corresponds to the e-folding decay (Caldwell et al. 1997) following $\varepsilon(t) = \varepsilon_* \exp(-t/\tau^*)$, with ε_* the daytime median value (black lines) and τ^* the convective timescale (~ 30 min). Dashed orange line represent fits of the e-folding decay for the same ε_* and adjusting for τ^* . This procedure yields $\tau_1^* = 5.5$ h and $\tau_2^* = 9.1$ h for each nighttime period. **(b)** ML thickness h_{mix} (blue bars). Daytime and nighttime averages are depicted by black lines and black dashed lines, respectively. The orange lines represent the evolution of h_{mix} during nighttime hours assuming a completely inactive ML, i.e., diffusivity smoothing out the ML without opposition (no convection). Following the ML-shape model (Φ_T), this situation can be accounted for by $h_{mix}(t) = h_{mix}^* - 4\delta$, with h_{mix}^* as the daytime average value and $\delta = \sqrt{4Kt}$. Data displayed (blue dots and bars) were obtained by averaging the resulting estimates from the profile as sampled by the two fast thermistors mounted on the VMP. Only sampled profiles that meet the Φ_T criteria were considered (including profiles with only one sample meeting the criteria).

sink if they stopped migrating upwards. Their sinking speed can be approximated as the Stokes sedimentation of a particle with ellipsoidal shape (Guazzelli and Morris 2011). Assuming sinking parallel to the main axis and rod-shaped dimensions as reported by Imhoff (2015), sinking speeds range from 0.01 to 0.02 mm s⁻¹ (Text S2 and Fig. S10). For context, their upward migration speed is of the same range (0.03 \pm 0.01 mm s⁻¹; Sommer et al. 2017). On the other hand, our measurements suggest a convective plume velocity $w^* = 0.37 \pm 0.25$ mm s⁻¹ (Table 2). This indicates that the convective plumes provide a vertical transport mechanism one order of magnitude more efficient than individual cell migration. This suggests that the generation of bioconvection during nighttime, although reduced and non-constant, considerably offsets the sinking rate of the bacterial community.

Critical bacterial concentration to trigger bioconvection. The stability ($N^2 = g\rho_0^{-1}\partial\rho/\partial z$) of the water–bacteria mixture in the ML can be analyzed to determine the minimal density contribution by bacteria for convective plumes to occur. Combining an unstable density profile given by $N^2 < 0$ with the water–bacteria mixture density ($\rho = \rho_w + \rho_{o\%}C_{Bac}$) and discretizing (forward finite difference) for the ML thickness, yields the following condition for bacterial concentration difference over the entire ML:

$$-\Delta C_{Bac} > \frac{h_{mix}}{g\xi} N_{ML}^2 \quad (10)$$

which leads to unstable density conditions. Here, $\Delta C_{Bac} = C_{Bac}^{down} - C_{Bac}^{up}$, where the superscripts indicate the upper and lower limits of the ML. Results presented in Table 2 give a $\Delta C_{Bac} = 7.5 \times 10^9 \text{ m}^{-3}$. Average bacterial concentration in the ML $C_{Bac}^{ML} = 1.3 \times 10^{11} \text{ m}^{-3}$ (Fig. S1) yields a difference of only 6% between the upper layer concentration and the necessary C_{Bac}^{ML} to induce convective plumes. Furthermore, considering data presented here and in Sommer et al. (2017) we find that $\Delta C_{Bac} \sim 10\%$ of C_{Bac}^{ML} , which translates to a 1–2 FTU difference in turbidity (see Fig. S1b for turbidity as a function of C_{Bac}). Such a difference in bacterial concentration is even more evident for the profiles collected in July 2017 (Fig. S9a), which show a peak maxima exceeding C_{Bac}^{ML} by ~ 5 FTU. Altogether, the present analysis suggests that the observed high concentrations of *C. okenii* generate favorable conditions for bioconvective plumes in Lake Cadagno.

Related phenomena in stratified waters. The vertical bacterial distributions shown in Fig. S9 resemble experimental studies, where intruding sediment-laden water has been overlaying sediment-free but denser water (Davaranpanah Jazi

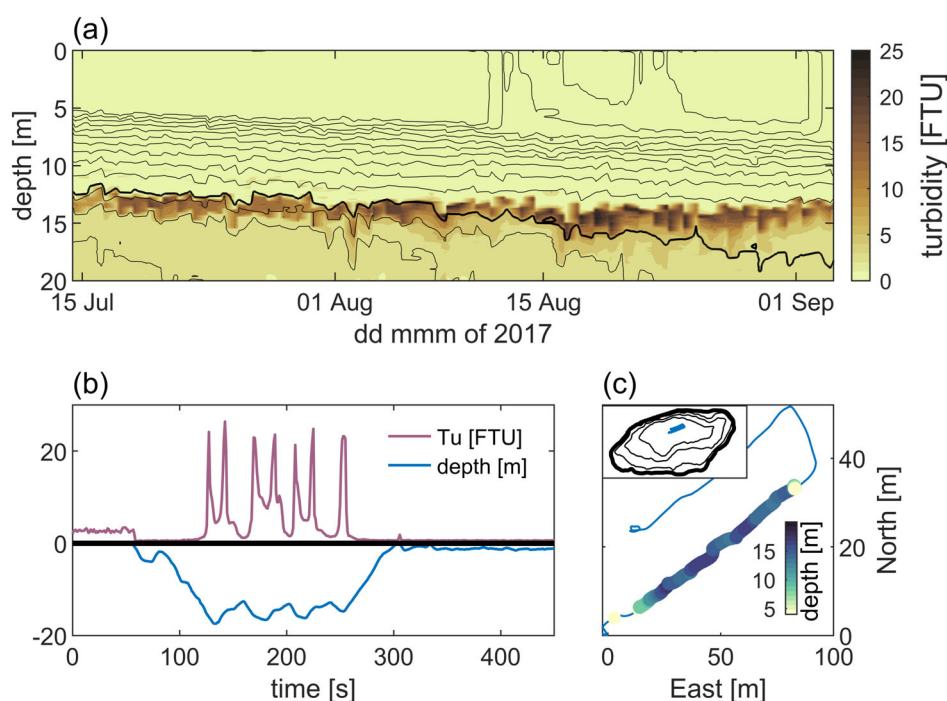


Fig 11. Seasonal and spatial persistence of the bacterial layer. **(a)** Time series of turbidity profile during summer 2017, as measured by the Sea & Sun 75M CTD. Thick black line corresponds to 5°C isothermal. Thin black lines above the thick black line represent isotherms from 15 to 6°C with 1°C decrement. Lines below correspond to 4.75, 4.50, and 4.25°C isotherms. All isotherms presented in **(a)** were obtained from the same CTD data. **(b)** Vertex AUV transect performed on the afternoon of 16 August 2017. The Y-axis is shared between turbidity (Tu [FTU]; positive) and depth (in m; negative; same scale). **(c)** Plan view of the AUV trajectory with distances measured from the sampling platform and depth color-code for positions below 4 m depth. Inset in **(c)** shows the AUV transect plan view within the lake. Thin black lines depict 5, 10, and 15 m depth bathymetric isolines.

and Wells 2016). Assuming that for this overall stable configuration the density difference between the sediment-laden upper layer and the sediment-free layer underneath is only marginal, two types of convection can occur. Double diffusion could establish if the molecular diffusion of the denser water components would reach high enough, so that the lower bound of the sediment-containing layer could become unstable and form sediment fingers (Burns and Meiburg 2015). Alternatively, settling sediment could locally enhance the density of the denser underlying water and thereby cause classical convective instabilities (figs. 1a,b in Davarpanah Jazi and Wells 2016). Whereas double diffusion could indeed form at the beginning of the season, when the bacteria concentrations are low and hence have little effect on the density, the second process seems unrealistic as *C. okenii* have to swim upward to remain in the ideal living environment of the water column, defined by a certain amount of light and H_2S . For the observations presented in this paper, the bacterial concentrations are, however, too high for double diffusion to be relevant.

Seasonal and spatial persistency. The process of bioconvection has been detected in Lake Cadagno during the summer months (Sommer et al. 2017; Sepúlveda Steiner et al. 2019). The present work details the temporal evolution

of a bacteria-induced ML maintained throughout a diel cycle and links records of this bacterial ML to turbidity. The question arises as to whether these measurements represent a transient, episodic or a systematic process. A bi-daily CTD profile monitoring performed during summer 2017 provides evidence of seasonal persistency (Fig. 11a). These measurements reveal a turbid layer located at ~12 to ~15 m depth and persisting throughout the entire density-stratified summer period. Furthermore, turbidity transects (Fig. 11b,c) performed in 2017 with an AUV (Hydromea-Vertex; Schill et al. 2018; Quraishi et al. 2018) documented spatial persistence of the bacterial layer along several tens of meters. Further research is needed to unravel the seasonal and spatial variability of the bioconvective ML. However, preliminary analyses presented in Fig. 11 provide compelling evidence that bioconvection occurs (1) throughout the summertime and (2) consistently below the chemocline over the entire lake.

Implications and remarks. Specifically, in Lake Cadagno, bioconvection expands the habitat of *C. okenii*, exposing the bacterial community to light and entraining H_2S from below. This suggests active participation in the creation of their ecological niche. We show here that the ML, representing the expanded habitat of these photoautotrophic bacteria, does not form every day at dawn but rather persists throughout

nighttime hours (Figs. 1, 5). Although reduced in comparison to daytime, our analysis shows that the bacteria remain active during nighttime (Figs. 9, 10). Further research can help resolve physiological/metabolic reasons for this behavior. We provide several physical hypotheses concerning the advantages of continuous vertical migration and resultant bioconvection.

Conclusions

In this study, we focused on the persistence of a mixed layer induced by bioconvection over the daily cycle in a natural lake system. Analyses from an intensive 48-h campaign, investigating the *C. okenii* bacterial layer in the alpine and meromictic Lake Cadagno (Switzerland) offer the following conclusions:

1. The competing effects of convection and turbulent diffusion can be inferred from in situ observations. The temporal evolution of highly resolved temperature profiles demonstrated the key role of biological activity in the water column dynamics.
2. Although the level of homogeneity of the bioconvective mixed layer (ML) varies over time, it persists throughout the diel cycle. This persistence seems to also apply on seasonal scales (during the whole summer) and on spatial scales (below the chemocline over the lateral extent of the whole lake).
3. Despite strong stratification during summer in Lake Cadagno, our observations suggest the presence of considerable diapycnal mixing adjacent to the bioconvective ML. The development of this homogeneous profile over the daily cycle is best explained by a continuation of bacterial migration during nighttime hours. Without upward migration, diapycnal mixing would dissolve the bio-convectively induced ML over the duration of one night.

Finally, we demonstrated with this study the possibility of drawing conclusions on the dynamics of specific biological phenomena, using solely in situ physical observational methods. Small to medium-sized lakes are characterized by low to moderate energetics, which can be accurately sensed with modern small-scale instrumentation, and are thereby ideal environments for further exploration.

References

- Abraham, E. R. 1998. The generation of plankton patchiness by turbulent stirring. *Nature* **391**: 577–580. doi:[10.1038/35361](https://doi.org/10.1038/35361)
- Baker, M. A., and C. H. Gibson. 1987. Sampling turbulence in the stratified ocean: Statistical consequences of strong intermittency. *J. Phys. Oceanogr.* **17**: 1817–1836. doi:[10.1175/1520-0485\(1987\)017<1817:STITSO>2.0.CO;2](https://doi.org/10.1175/1520-0485(1987)017<1817:STITSO>2.0.CO;2)
- Batchelor, G. K. 1959. Small-scale variation of convected quantities like temperature in turbulent fluid Part 1. General discussion and the case of small conductivity. *J. Fluid Mech.* **5**: 113–133. doi:[10.1017/S002211205900009X](https://doi.org/10.1017/S002211205900009X)
- Beaton, R. N., and D. Grünbaum. 2006. Bioconvection in a stratified environment: Experiments and theory. *Phys. Fluids* **18**: 127102. doi:[10.1063/1.2402490](https://doi.org/10.1063/1.2402490)
- Bees, M. A. 2020. Advances in bioconvection. *Annu. Rev. Fluid Mech.* **52**: 449–476. doi:[10.1146/annurev-fluid-010518-040558](https://doi.org/10.1146/annurev-fluid-010518-040558)
- Bees, M. A., and N. A. Hill. 1997. Wavelengths of bioconvection patterns. *J. Exp. Biol.* **200**: 1515–1526.
- Berg, J. S., and others. 2019. Dark aerobic sulfide oxidation by anoxygenic phototrophs in anoxic waters. *Environ. Microbiol.* **21**: 1611–1626. doi:[10.1111/1462-2920.14543](https://doi.org/10.1111/1462-2920.14543)
- Boehrer, B., and M. Schultze. 2008. Stratification of lakes. *Rev. Geophys.* **46**: RG2005. doi:[10.1029/2006RG000210](https://doi.org/10.1029/2006RG000210)
- Burns, P., and E. Meiburg. 2015. Sediment-laden fresh water above salt water: nonlinear simulations. *J. Fluid Mech.* **762**: 156–195. doi:[10.1017/jfm.2014.645](https://doi.org/10.1017/jfm.2014.645)
- Caldwell, D. R., R.-C. Lien, J. N. Moum, and M. C. Gregg. 1997. Turbulence decay and restratification in the equatorial ocean surface layer following nighttime convection. *J. Phys. Oceanogr.* **27**: 1120–1132. doi:[10.1175/1520-0485\(1997\)027<1120:TDARIT>2.0.CO;2](https://doi.org/10.1175/1520-0485(1997)027<1120:TDARIT>2.0.CO;2)
- Culver, D. A. 1977. Biogenic meromixis and stability in a soft-water lake. *Limnol. Oceanogr.* **22**: 667–686. doi:[10.4319/lo.1977.22.4.0667](https://doi.org/10.4319/lo.1977.22.4.0667)
- Danza, F., D. Ravasi, N. Storelli, S. Roman, S. Lüdin, M. Bueche, and M. Tonolla. 2018. Bacterial diversity in the water column of meromictic Lake Cadagno and evidence for seasonal dynamics. *PLoS One* **13**: e0209743. doi:[10.1371/journal.pone.0209743](https://doi.org/10.1371/journal.pone.0209743)
- Danza, F., N. Storelli, S. Roman, S. Lüdin, and M. Tonolla. 2017. Dynamic cellular complexity of anoxygenic phototrophic sulfur bacteria in the chemocline of meromictic Lake Cadagno. *PLoS One* **12**: e0189510. doi:[10.1371/journal.pone.0189510](https://doi.org/10.1371/journal.pone.0189510)
- Davarpanah Jazi, S., and M. G. Wells. 2016. Enhanced sedimentation beneath particle-laden flows in lakes and the ocean due to double-diffusive convection. *Geophys. Res. Lett.* **43**: 10,883–10,890. doi:[10.1002/2016GL069547](https://doi.org/10.1002/2016GL069547)
- Davies Wykes, M. S., G. O. Hughes, and S. B. Dalziel. 2015. On the meaning of mixing efficiency for buoyancy-driven mixing in stratified turbulent flows. *J. Fluid Mech.* **781**: 261–275. doi:[10.1017/jfm.2015.462](https://doi.org/10.1017/jfm.2015.462)
- Deardorff, J. W. 1970. Convective velocity and temperature scales for the unstable planetary boundary layer and for Rayleigh convection. *J. Atmos. Sci.* **27**: 1211–1213. doi:[10.1175/1520-0469\(1970\)027<1211:CVATSF>2.0.CO;2](https://doi.org/10.1175/1520-0469(1970)027<1211:CVATSF>2.0.CO;2)
- Del Don, C., K. W. Hanselmann, R. Peduzzi, and R. Bachofen. 2001. The meromictic alpine Lake Cadagno: Orographical and biogeochemical description. *Aquat. Sci.* **63**: 70–90. doi:[10.1007/PL00001345](https://doi.org/10.1007/PL00001345)
- Dufois, F., N. J. Hardman-Mountford, J. Greenwood, A. J. Richardson, M. Feng, and R. J. Matear. 2016. Anticyclonic eddies are more productive than cyclonic eddies in

- subtropical gyres because of winter mixing. *Sci. Adv.* **2**: e1600282. doi:[10.1126/sciadv.1600282](https://doi.org/10.1126/sciadv.1600282)
- Durham, W. M., and R. Stocker. 2012. Thin phytoplankton layers: Characteristics, mechanisms, and consequences. *Ann. Rev. Mar. Sci.* **4**: 177–207. doi:[10.1146/annurev-marine-120710-100957](https://doi.org/10.1146/annurev-marine-120710-100957)
- Egli, K., M. Wiggli, M. Fritz, J. Klug, J. Gerss, and R. Bachofen. 2004. Spatial and temporal dynamics of a plume of phototrophic microorganisms in a meromictic alpine lake using turbidity as a measure of cell density. *Aquat. Microb. Ecol.* **35**: 105–113. doi:[10.3354/ame035105](https://doi.org/10.3354/ame035105)
- Fischer, C., M. Wiggli, F. Schanz, K. W. Hanselmann, and R. Bachofen. 1996. Light environment and synthesis of bacteriochlorophyll by populations of *Chromatium okenii* under natural environmental conditions. *FEMS Microbiol. Ecol.* **21**: 1–9. doi:[10.1016/0168-6496\(96\)00037-2](https://doi.org/10.1016/0168-6496(96)00037-2)
- Guazzelli, E., and J. F. Morris. 2011. A physical introduction to suspension dynamics. Cambridge University Press.
- Hill, N. A., and T. J. Pedley. 2005. Bioconvection. *Fluid Dyn. Res.* **37**: 1–20. doi:[10.1016/j.fluiddyn.2005.03.002](https://doi.org/10.1016/j.fluiddyn.2005.03.002)
- Houghton, I. A., J. R. Koseff, S. G. Monismith, and J. O. Dabiri. 2018. Vertically migrating swimmers generate aggregation-scale eddies in a stratified column. *Nature* **556**: 497–500. doi:[10.1038/s41586-018-0044-z](https://doi.org/10.1038/s41586-018-0044-z)
- Imhoff, J. F. 2015. *Chromatium*. In *Bergey's manual of systematics of archaea and bacteria*. John Wiley & Sons, Ltd.
- Ivey, G. N., K. B. Winters, and J. R. Koseff. 2008. Density stratification, turbulence, but how much mixing? *Annu. Rev. Fluid Mech.* **40**: 169–184. doi:[10.1146/annurev.fluid.39.050905.110314](https://doi.org/10.1146/annurev.fluid.39.050905.110314)
- János, I. M., J. O. Kessler, and V. K. Horváth. 1998. Onset of bioconvection in suspensions of *Bacillus subtilis*. *Phys. Rev. E* **58**: 4793–4800. doi:[10.1103/PhysRevE.58.4793](https://doi.org/10.1103/PhysRevE.58.4793)
- Jonas, T., A. Stips, W. Eugster, and A. Wüest. 2003. Observations of a quasi shear-free lacustrine convective boundary layer: Stratification and its implications on turbulence. *J. Geophys. Res.* **108**: 3328. doi:[10.1029/2002JC001440](https://doi.org/10.1029/2002JC001440)
- Kunze, E. 2019. Biologically generated mixing in the ocean. *Ann. Rev. Mar. Sci.* **11**: 215–226. doi:[10.1146/annurev-marine-010318-095047](https://doi.org/10.1146/annurev-marine-010318-095047)
- Kunze, E., J. F. Dower, I. Beveridge, R. Dewey, and K. P. Bartlett. 2006. Observations of biologically generated turbulence in a coastal inlet. *Science* **313**: 1768–1770. doi:[10.1126/science.1129378](https://doi.org/10.1126/science.1129378)
- Lévy, M., P. J. S. Franks, and K. S. Smith. 2018. The role of submesoscale currents in structuring marine ecosystems. *Nat. Commun.* **9**: 4758. doi:[10.1038/s41467-018-07059-3](https://doi.org/10.1038/s41467-018-07059-3)
- Lorenzen, C. J. 1972. Extinction of light in the ocean by phytoplankton. *ICES J. Mar. Sci.* **34**: 262–267. doi:[10.1093/icesjms/34.2.262](https://doi.org/10.1093/icesjms/34.2.262)
- Lorke, A., and W. N. Probst. 2010. In situ measurements of turbulence in fish shoals. *Limnol. Oceanogr.* **55**: 354–364. doi:[10.4319/lo.2010.55.1.0354](https://doi.org/10.4319/lo.2010.55.1.0354)
- Luedin, S. M., and others. 2019. Draft genome sequence of *Chromatium okenii* isolated from the stratified alpine Lake Cadagno. *Sci. Rep.* **9**: 1936. doi:[10.1038/s41598-018-38202-1](https://doi.org/10.1038/s41598-018-38202-1)
- Luketina, D. A., and J. Imberger. 2001. Determining turbulent kinetic energy dissipation from Batchelor curve fitting. *J. Atmos. Ocean. Technol.* **18**: 100–113. doi:[10.1175/1520-0426\(2001\)018<0100:DTKEDF>2.0.CO;2](https://doi.org/10.1175/1520-0426(2001)018<0100:DTKEDF>2.0.CO;2)
- Münnich, M., A. Wüest, and D. M. Imboden. 1992. Observations of the second vertical mode of the internal seiche in an alpine lake. *Limnol. Oceanogr.* **37**: 1705–1719. doi:[10.4319/lo.1992.37.8.1705](https://doi.org/10.4319/lo.1992.37.8.1705)
- Ng, S. M. Y. Y., J. P. Antenucci, M. R. Hipsey, G. Tibor, and T. Zohary. 2011. Physical controls on the spatial evolution of a dinoflagellate bloom in a large lake. *Limnol. Oceanogr.* **56**: 2265–2281. doi:[10.4319/lo.2011.56.6.2265](https://doi.org/10.4319/lo.2011.56.6.2265)
- Noss, C., and A. Lorke. 2014. Direct observation of biomixing by vertically migrating zooplankton. *Limnol. Oceanogr.* **59**: 724–732. doi:[10.4319/lo.2014.59.3.0724](https://doi.org/10.4319/lo.2014.59.3.0724)
- Osborn, T. R. 1980. Estimates of the local rate of vertical diffusion from dissipation measurements. *J. Phys. Oceanogr.* **10**: 83–89. doi:[10.1175/1520-0485\(1980\)010<0083:EOTLRO>2.0.CO;2](https://doi.org/10.1175/1520-0485(1980)010<0083:EOTLRO>2.0.CO;2)
- Osborn, T. R., and C. S. Cox. 1972. Oceanic fine structure. *Geophys. Fluid Dyn.* **3**: 321–345. doi:[10.1080/03091927208236085](https://doi.org/10.1080/03091927208236085)
- Oschlies, A., and V. Garçon. 1998. Eddy-induced enhancement of primary production in a model of the North Atlantic Ocean. *Nature* **394**: 266–269. doi:[10.1038/28373](https://doi.org/10.1038/28373)
- Quraishi, A., A. Bahr, F. Schill, and A. Martinoli. 2018. Autonomous feature tracing and adaptive sampling in real-world underwater environments. *2018 IEEE International Conference on Robotics and Automation (ICRA)*. IEEE. 5699–5704.
- Ruddick, B., A. Anis, and K. Thompson. 2000. Maximum likelihood spectral fitting: The Batchelor spectrum. *J. Atmos. Ocean. Technol.* **17**: 1541–1555. doi:[10.1175/1520-0426\(2000\)017<1541:MLSFTB>2.0.CO;2](https://doi.org/10.1175/1520-0426(2000)017<1541:MLSFTB>2.0.CO;2)
- Sathyendranath, S., A. D. Gouveia, S. R. Shetye, P. Ravindran, and T. Platt. 1991. Biological control of surface temperature in the Arabian Sea. *Nature* **349**: 54–56. doi:[10.1038/349054a0](https://doi.org/10.1038/349054a0)
- Schanz, F. 1985. Vertical light attenuation and phytoplankton development in Lake Zürich. *Limnol. Oceanogr.* **30**: 299–310. doi:[10.4319/lo.1985.30.2.0299](https://doi.org/10.4319/lo.1985.30.2.0299)
- Schanz, F., C. Fischer-Romero, and R. Bachofen. 1998. Photosynthetic production and photoadaptation of phototrophic sulfur bacteria in Lake Cadagno (Switzerland). *Limnol. Oceanogr.* **43**: 1262–1269. doi:[10.4319/lo.1998.43.6.1262](https://doi.org/10.4319/lo.1998.43.6.1262)
- Schill, F., A. Bahr, and A. Martinoli. 2018. Vertex: A new distributed underwater robotic platform for environmental monitoring, Distributed autonomous robotic systems, p. 679–693. In R. Groß, A. Kolling, S. Berman, E. Frazzoli, A. Martinoli, F. Matsuno, and G. Melvin [eds.], Springer proceedings in advanced robotics, v. **6**. Cham: Springer.

- Sepúlveda Steiner, O., D. Bouffard, and A. Wüest. 2019. Convection-diffusion competition within mixed layers of stratified natural waters. *Geophys. Res. Lett.* **46**: 13199–13208. doi:[10.1029/2019GL085361](https://doi.org/10.1029/2019GL085361)
- Simoncelli, S., S. J. Thackeray, and D. J. Wain. 2018. On biogenic turbulence production and mixing from vertically migrating zooplankton in lakes. *Aquat. Sci.* **80**: 35. doi:[10.1007/s00027-018-0586-z](https://doi.org/10.1007/s00027-018-0586-z)
- Sommer, T., J. R. Carpenter, M. Schmid, R. G. Lueck, and A. Wüest. 2013. Revisiting microstructure sensor responses with implications for double-diffusive fluxes. *J. Atmos. Ocean. Technol.* **30**: 1907–1923. doi:[10.1175/JTECH-D-12-00272.1](https://doi.org/10.1175/JTECH-D-12-00272.1)
- Sommer, T., and others. 2017. Bacteria-induced mixing in natural waters. *Geophys. Res. Lett.* **44**: 9424–9432. doi:[10.1002/2017GL074868](https://doi.org/10.1002/2017GL074868)
- Steinbuck, J. V., M. T. Stacey, M. A. McManus, O. M. Cheriton, and J. P. Ryan. 2009a. Observations of turbulent mixing in a phytoplankton thin layer: Implications for formation, maintenance, and breakdown. *Limnol. Oceanogr.* **54**: 1353–1368. doi:[10.4319/lo.2009.54.4.1353](https://doi.org/10.4319/lo.2009.54.4.1353)
- Steinbuck, J. V., M. T. Stacey, and S. G. Monismith. 2009b. An evaluation of χ^2 estimation techniques: Implications for Batchelor fitting and ϵ . *J. Atmos. Ocean. Technol.* **26**: 1652–1662. doi:[10.1175/2009JTECHO611.1](https://doi.org/10.1175/2009JTECHO611.1)
- Strutton, P. G., and F. P. Chavez. 2004. Biological heating in the equatorial Pacific: Observed variability and potential for real-time calculation. *J. Clim.* **17**: 1097–1109. doi:[10.1175/1520-0442\(2004\)017<1097:BHITEP>2.0.CO;2](https://doi.org/10.1175/1520-0442(2004)017<1097:BHITEP>2.0.CO;2)
- Thorpe, S. A. 1977. Turbulence and mixing in a Scottish Loch. *Philos. Trans. R. Soc. A Math. Phys. Eng. Sci.* **286**: 125–181. doi:[10.1098/rsta.1977.0112](https://doi.org/10.1098/rsta.1977.0112)
- Tonolla, M., A. Demarta, R. Peduzzi, and D. Hahn. 1999. In situ analysis of phototrophic sulfur bacteria in the chemocline of meromictic Lake Cadagno (Switzerland). *Appl. Environ. Microbiol.* **65**: 1325–1330.
- Turner, J. S. 1973. Buoyancy effects in fluids. Cambridge University Press.
- Uhde, M., 1992. Mischungsprozesse im Hypolimnion des meromiktischen Lago Cadagno: Eine Untersuchung mit Hilfe natürlicher und künstlicher Tracer. Master Thesis, University of Freiburg, Germany.
- Viaroli, P., and others. 2018. Persistence of meromixis and its effects on redox conditions and trophic status in Lake Idro (Southern Alps, Italy). *Hydrobiologia* **824**: 51–69. doi:[10.1007/s10750-018-3767-9](https://doi.org/10.1007/s10750-018-3767-9)
- Weimer, W. C., and F. F. Lee. 1973. Some considerations of the chemical limnology of meromictic Lake Mary. *Limnol. Oceanogr.* **18**: 414–425. doi:[10.4319/lo.1973.18.3.0414](https://doi.org/10.4319/lo.1973.18.3.0414)
- Weiss, R. F., E. C. Carmack, and V. M. Koropalov. 1991. Deep-water renewal and biological production in Lake Baikal. *Nature* **349**: 665–669. doi:[10.1038/349665a0](https://doi.org/10.1038/349665a0)
- Wüest, A. 1994. Interactions in lakes: Biology as source of dominant physical forces. *Limnologia* **24**: 93–104.
- Wüest, A., G. Piepke, and J. D. Halfman. 1996, 202. Combined effects of dissolved solids and temperature on the density stratification of Lake Malawi (East Africa), p. 183. In T. C. Johnson and E. O. Odada [eds.], *The limnology, climatology and paleoclimatology of the East African Lakes*. New York: Gordon and Breach Scientific Publishers.
- Wüest, A., G. Piepke, and D. C. Van Senden. 2000. Turbulent kinetic energy balance as a tool for estimating vertical diffusivity in wind-forced stratified waters. *Limnol. Ocean.* **45**: 1388–1400. doi:[10.4319/lo.2000.45.6.1388](https://doi.org/10.4319/lo.2000.45.6.1388)

Acknowledgements

We thank Piora Centro Biologia Alpina (CBA) for use of the sampling platform and housing as well as Samuele Roman for logistical support. We acknowledge our technical staff, Sébastien Lavanchy (EPFL) and Michael Plüss (Eawag) for their contribution to the design of the HR-mooring, installation of instruments and the weather station, and their help in the profiling campaign. We are grateful to Angelo Carlino, Hannah Chmiel, Cintia Ramón Casañas, Love Råman Vinnå and Tomy Doda for their assistance during fieldwork. Valuable feedback from Helmut Bürgmann on dark metabolic pathways helped to improve the manuscript's discussion. Bieito Fernández-Castro, Hugo Ulloa, Camille Minaudo and Cary Troy provided helpful discussions on various physical aspects. Nicola Storelli and Mauro Tonolla (SUPSI) kindly provided profiles of *C. okenii* concentrations and turbidity measurements used in Fig. S1. Emilie Haizmann and Angelo Carlino collected the 2017 seasonal CTD dataset. We are grateful for their outstanding commitment. We are thankful to Anwar Quraishi and Alcherio Martinoli of the Distributed Intelligent Systems and Algorithms Laboratory (DISAL) at EPFL, and Alexander Bahr and Felix Schill from Hydromea S.A. for their collaboration and for the collection of the AUV data. Rich Pawlowicz's m_map v1.4k Matlab toolbox (<https://www.eoas.ubc.ca/~rich/map>) was used to plot Fig. 2a. The first author appreciates efforts to keep the toolbox and its supporting website updated. Comments and suggestions from two anonymous reviewers and the Associate Editor helped to improve this manuscript.

This work was financed by the Swiss National Science Foundation—Sinergia grant CRSII2_160726 (*A Flexible Underwater Distributed Robotic System for High-Resolution Sensing of Aquatic Ecosystems*).

Conflict of Interest

None declared.

Submitted 03 March 2020

Revised 09 October 2020

Accepted 30 December 2020

Associate editor: Sally MacIntyre